Functional Modules of KdpB, the Catalytic Subunit of the Kdp-ATPase from *Escherichia coli*†

Marc Bramkamp§ and Karlheinz Altendorf*

Universität Osnabrück, Fachbereich Biologie/Chemie, Abteilung Mikrobiologie, D-49069 Osnabrück, Germany

Received June 18, 2004; Revised Manuscript Received July 6, 2004

ABSTRACT: The large cytoplasmic domain (H4H5) of KdpB of the KdpFABC complex (P-type ATPase) from *Escherichia coli* consists of two separate modules, the phosphorylation domain (KdpBP) and the nucleotide binding domain (KdpBN). The H4H5 and the KdpBN domains were purified as soluble 10His-tagged fusion proteins. Both proteins exhibit a mainly α-helical secondary structure as judged by CD spectroscopy. Fluorescein 5-isothiocyanate (FITC) labeling studies revealed that both proteins form a proper nucleotide binding site. Adenosine nucleotides protect the H4H5 loop but not KdpBN against FITC modification. Trinitrophenyl (TNP)-nucleotide binding studies revealed that both H4H5 and KdpBN bind nucleotides with high affinity. Furthermore, the H4H5 loop was still able to hydrolyze ATP, as well as *p*-nitrophenyl phosphate (pNPP). These results lend support to the notion that the separately synthesized H4H5 and KdpBN domains retain their native structure and that they reveal properties of both P2-type ATPases (e.g., Na^+,K^+-ATPase and Ca^{2+}-ATPase) and P1b-type ATPases (e.g., heavy metal transporting ATPases). Furthermore, this report also emphasizes the unique position of the Kdp-ATPase within the P-type ATPase family.

Maintenance of cell turgor is a vital prerequisite for the life of prokaryotic cells. Since in most cases K^+ ions play a major role in that process (*1*), bacteria, such as *Escherichia coli*, have established a variety of K^+ influx and efflux systems (for review, see ref *2*). Under potassium-limiting conditions (K^+ >1 mM) or high osmolality in the medium, the expression of the *kdpFABC* operon, coding for a high-affinity (K_M = 2 μM) K^+ uptake system (KdpFABC complex), is induced in *Escherichia coli* (*3*). Thus, the KdpFABC complex is synthesized as an emergency system when other K^+ uptake systems cannot meet the need of the cells for K^+ ions (*4*, *5*). The enzyme complex is a member of the P-type ATPase family, members of which are found in all kingdoms of life and which transport a variety of charged substrates across the membrane. Their substrate specificity led to a classification into different subgroups (*6, 7*). Among the P-type ATPases, the KdpFABC complex exhibits a rather unique subunit composition (for review, see refs *7*−*9*). While in all known P-type ATPases the catalytic activity and transport capacity are located on the same subunit, these features are found on separate polypeptides in the case of the Kdp-ATPase.[1] The catalytic subunit KdpB, which is phosphorylated during the reaction cycle (*10*) at the aspartate residue 307 (*11*), shares the conserved regions, first summarized by Serrano, with other P-type ATPases (*12*). Ion transport is mediated by the KdpA subunit, which shares some homologies with potassium channels, such as the well characterized bacterial KcsA channel from *Streptomyces lividans* (*13, 14*). Mutational analysis of KdpA supports the notion that KdpA has two or four selectivity filters and P-loop regions (*15*−*17*).

Most of the studies on structure−function relationship have been carried out with eukaryotic P-type ATPases, for example, the Na^+,K^+-ATPase, the Ca^{2+}-ATPase, the H^+,K^+-ATPase, and the H^+-ATPase. The recent elucidation of the structure of the sarcoplasmatic/endoplasmatic reticulum Ca^{2+}-ATPase (*18, 19*) was a cornerstone in understanding the structure and the transport mechanism of P-type ATPases. To obtain structural information also for the Kdp-ATPase, a member of a unique class of P-type ATPases, as a first step toward this goal the cytoplasmic domains of the KdpB subunit were characterized. The large cytoplasmic loop located between helix four and helix five (therefore called the H4H5 loop) contains the phosphorylation site and the nucleotide binding site. The architecture of the H4H5 loop is similar in all P-type ATPases, and amino acids within the loop have been identified for ATP binding and phosphorylation. The crystal structure of the Ca^{2+}-ATPase confirmed that the H4H5 loop consists of two separate domains, the

† Support for this study was provided by the Deutsche Forschungsgemeinschaft (Grant SPP 1070) and the Fonds der Chemischen Industrie (fellowship to M.B.).

* Corresponding author. Address: Universität Osnabrück, Fachbereich Biologie/Chemie, Abteilung Mikrobiologie, D-49069 Osnabrück, Germany. Tel: +49(0)541-9692864. Fax: +49(0)541-96912891. E-mail: altendorf@biologie.uni-osnabrueck.de.

§ Current address: Sir William Dunn School of Pathology, University of Oxford, South Parks Road, Oxford OX1 3RE, U.K.

[1] Abbreviations: AMP-PNP, 5′-adenylimido diphosphate; BSA, bovine serum albumin; CNBr, cyanogen bromide; DMSO, dimethyl sulfoxide; FITC, fluorescein 5-isothiocyanate; Kdp, potassium-dependent adenosine triphosphatase (E. C. 3.6.1.36); Na^+,K^+-ATPase (sodium pump), sodium−potassium-transporting adenosine triphosphatase; pNPP, *p*-nitrophenyl phosphate; P_i, inorganic phosphate; PAGE, polyacrylamide gel electrophoresis; SERCA (calcium pump, Ca^{2+}-ATPase), sarcoplasmic calcium-transporting adenosine triphosphatase; SDS, sodium dodecyl sulfate; TNP-ATP, 2′- (or 3′-) O-(trinitrophenyl)-adenosine 5′-triphosphate.

10.1021/bi048727d CCC: $27.50
Published on Web 09/03/2004

phosphorylation domain and the nucleotide binding domain. While the phosphorylation domain is a classical Rossman fold and its architechture is probably similar in all P-type ATPases, the heavy metal transporting P-type ATPases, the H^+-ATPase, and the KdpB protein have a much smaller (around 100 amino acids) nucleotide binding domain compared to other P-type ATPases.

In this report, the overproduction of the H4H5 loop and the nucleotide binding domain (KdpBN) of the KdpB subunit are described. We found that the H4H5 loop still binds and hydrolyzes ATP and pNPP, whereas the KdpBN domain has only maintained the capacity to bind nucleotides.

EXPERIMENTAL PROCEDURES

Materials. All chemicals were of analytical grade. All nucleotides and fluorescein 5-isothiocyanate isomer I were purchased from Sigma. *p*-Nitrophenyl phosphate was from ICN Biomedical Research Products. Protein molecular mass standard was purchased from NOVEX.

Bacterial Strains and Plasmids. The *E. coli* BL21(DE3)/pLysS strain was obtained from Novagen and transformed with pET16b derivatives carrying the coding regions for the H4H5 loop and the KdpBN domain. The resulting transformants were grown in Luria−Bertani (LB) medium containing 50 μg mL^{-1} ampicillin and 30 μg mL^{-1} chloramphenicol.

SDS−Polyacrylamide Gel Electrophoresis. The separation of proteins was carried out by SDS−PAGE according to Laemmli (*20*). Protein samples were mixed with SDS sample buffer before loading onto the gel (*20*). The standard acrylamide concentration was 14%. The gels were stained with silver according to the procedure of Blum et al. (*21*) or with Coomassie blue (*22*).

Cloning of the H4H5 Loop and the KdpBN Domain. The coding regions of the H4H5 loop and the KdpBN domain of *kdpB* were amplified using the polymerase chain reaction (PCR) with the pSM5 plasmid, which carries the *kdpFABC* operon of *E. coli*, as a template. The oligonucleotide primers used in the PCR reaction were as follows: H4H5 for, 5′-CATATGCTAGGCGCGAATGTGATT-3′; H4H5 rev, 5′-GGATCCTTACTATTACTGTTTGCCAATGTGCAC-3′; KdpBN for, 5′-ACACATATGAACCGTCAGGCGTCGGAG-3′; KdpBN rev, 5′-GCGCTCGAGCTATTAGCCTTTGACGATATCTTTCAG-3′. All primers were purchased from MWG Biotech. The forward primers produce a *Nde*I site and the H4H5 reverse primer builds a *Bam*HI restriction site, while the KdpBN reverse primer contains a *Xho*I site (restriction sites are underlined). Resulting PCR products were cloned in the pUC18 vector and transformed into DH5α cells. The sequences were analyzed by cycle sequencing. The constructs were digested with the appropriate restriction endonucleases and cloned into pET16b vectors. The resulting plasmids pET16bH4H5 and pET16bKdpBN were transformed into BL21(DE3)/pLysS cells.

Overproduction of H4H5 and KdpBN. Cloning within the *Nde*I site of pET16b results in a fusion protein carrying a 10 histidine motif and a 10 amino acid linker at the N terminus of the desired protein. For the synthesis of H4H5, BL21(DE3) cells were grown in LB medium at 37 °C in 50 mL culture flasks until an OD_{600} of around 1.0 was reached. The cells were than shifted to 30 °C, and 1 mM IPTG was added. Three hours later the cells were harvested. Production of the KdpBN protein in BL21(DE3) cells was carried out in 50 mL flasks or in a 5 L Biostad M fermenter. Since the formation of inclusion bodies was not observed, cells remained at 37 °C when 1 mM IPTG was added.

Purification of the 10His-Tagged H4H5 and KdpBN Proteins. Cells in buffer A containing 40 mM Tris/HCl, pH 7.8, 10 mM imidazole, 150 mM NaCl, 1 μg mL^{-1} DNase, and one tablet of Roche Complete protease inhibitor per 50 mL were passed through a Ribi cell fractionator with a pressure of 20 000 psi. The cell lysate was centrifuged in an ultracentrifuge at 100 000 × *g*, and the supernatant was transferred to a Ni−NTA slurry equilibrated with buffer A. Binding occurred at 4 °C for 1 h under permanent shaking. The Ni−NTA material was than collected by centrifugation and washed three times with buffer B (40 mM Tris/HCl, pH 7.8, 60 mM imidazole, and 150 mM NaCl). Elution of the H4H5 or KdpBN proteins was carried out in buffer C containing 40 mM Tris/HCl, pH 7.8, 0.5 M imidazole, and 100 mM NaCl. Protein concentrations were determined using the BCA assay from Pierce for the H4H5 protein. Since KdpBN lacks amino acids necessary for using the BCA assay, the Bio-Rad protein assay according to Bradford was applied. If necessary, the proteins were concentrated using an Amicon cell (Amicon, Millipore).

FITC Modification. FITC modification of either the KdpFABC complex (purified by the method of Siebers et al. (*23*)), the H4H5 loop, and the KdpBN domain was carried out using 10 μg of protein in buffer containing 25 mM Tris/HCl, pH 9.2, 150 mM choline chloride, 12.5 mM histidine, and 1 mM $MgCl_2$. Routinely, 15 μg of FITC were used for labeling experiments, and the reaction was carried out in the dark using black tubes at 37 °C for 30 min. The influence of nucleotides was tested by adding 5 mM of the desired nucleotide 5 min prior FITC addition. To test binding of FITC to unfolded proteins, the KdpFABC complex, the H4H5 loop, and the KdpBN domain were treated with 1% SDS at 80 °C for 10 min. The labeled proteins were separated on Laemmli gels, and FITC fluorescence was visualized under UV light (366 nm). The gels were then stained with Coomassie brilliant blue.

Circular Dichroism Spectroscopy. CD spectra were collected at room temperature on a Jasco J-600 spectropolarimeter equipped with a 0.1 mm path length cell. For each data set, 50 spectra were acquired at a scan speed of 50 nm min^{-1} with a step resolution of 1 nm. Spectra were corrected using the corresponding buffer spectra. The proteins were dialyzed against 50 mM potassium phosphate buffer, pH 7.5, and the protein concentrations used were between 0.5 (H4H5) and 2 mg mL^{-1} (KdpBN).

ATPase Activity. For the determination of the ATPase activity of the purified H4H5 loop, the EnzCheck phosphate assay from Molecular Probes was used. The production of the 2-amino-6-mercapto-7-methylpurine was followed spectroscopically at 360 nm at room temperature. The protein concentrations used were 50 μg mL^{-1}. The reaction was carried out in a 1 mL cuvette, and the absorption change was measured continuously. The nonenzyme control was measured in the same way to determine the autohydrolysis of ATP.

Phosphatase Activity. The phosphatase activity of the purified H4H5 loop was measured using a microtiter assay as previously described (*24*). The total reaction volume was

100 μL containing 20 mM HEPES/Tris, pH 7.8, 15 mM $MgCl_2$, and 50 μg mL^{-1} protein. The mixture was preincubated at 37 °C for 5 min, and the reaction was started by adding 15 mM *p*-nitrophenyl phosphate. After 15 min at 37 °C, the reaction was stopped with 0.1 M NaOH. The reaction product *p*-nitrophenolate was immediately measured in an ELISA reader at 410 nm. The ELISA reader was calibrated with a water blank to give the results as true extinction values. The total amount of released *p*-nitrophenolate was calculated by using the extinction coefficient of $\epsilon = 18.5 \times 10^{-3}$ M^{-1} cm^{-1}. Each data point is an average out of duplicates. As controls, duplicates of the nonenzyme control values were subtracted from each data point. The effect of *ortho*-vanadate was measured by preincubation for 5 min at 37 °C.

TNP-Nucleotide Binding to H4H5 and KdpBN. Binding of TNP-ATP, TNP-ADP, and TNP-AMP to the H4H5 loop and the KdpBN domain was carried out in quartz cuvettes using a SLM Aminco spectrofluorimeter (SLM Instruments). The excitation wavelength was 408 nm (8 nm width), and the emission wavelength was 545 nm (8 nm width). The reaction was carried out in 1 mL of 20 mM HEPES/Tris, pH 7.8, and 5 μM enzyme. In case of the H4H5 loop, 80 mM imidazole was added. The TNP-nucleotides (TNP-ATP, TNP-ADP, TNP-AMP) were titrated from a 1 mM stock solution to obtain concentrations between 0 and 25 μM with a volume increase of less than 10%. The temperature was kept constant at 25 °C, and fluorescence measured in buffer was used as a blank. Denatured protein was used as a control for unspecific binding. The data were fitted using the following equation: (a[TNP-nucleotide]/(b + [TNP-nucleotide]) with a representing the maximum fluorescence change and b the apparent K_d.

To determine the apparent affinity constants (K_d) for ATP, ADP, and AMP, competition experiments with TNP-nucleotides were performed. The proteins (5 μM) were preincubated with 5 μM TNP-ATP in 20 mM HEPES/Tris, and the fluorescence level obtained was set to 100%. Subsequently, bound TNP-ATP was chased by titration with ATP (ADP, AMP). The decrease in fluorescence was recorded. The fluorescence background of unbound TNP-nucleotides was subtracted, and data were standardized. For every different nucleotide concentration, the titration curve was plotted and fitted to determine the apparent K_d value for the given nucleotide.

RESULTS

Overproduction and Purification of the H4H5 Loop and the KdpBN Domain. To assign different biochemical functions to either the intact H4H5 loop or the nucleotide binding domain KdpBN of KdpB, both proteins were separately synthesized in *E. coli* BL21(DE3) cells. Synthesis of the recombinant H4H5 loop was carried out in 50 mL cultures since upscale experiments to 1 or 5 L fermenter cultures resulted in massive degradation of the H4H5 protein. This degradation must occur within the cells prior to disruption, since addition of a variety of protease inhibitors did not prevent degradation. Analysis of whole cell extracts by SDS−PAGE supported this notion. Lowering the temperature from 37 to 30 °C prior induction with 1 mM IPTG minimized the formation of inclusion bodies, and almost all H4H5 protein was found in the soluble fraction. The time course of protein synthesis was monitored by immunoblotting using either the His-tag antibodies from Qiagen or polyclonal antibodies against KdpB. Optimal protein synthesis was observed 3 h after induction. Purification of the proteins was achieved by Ni−NTA affinity chromatography and monitored by applying aliquots from each purification step to SDS−PAGE. Figure 1 shows the results for the recombinant H4H5 loop and Figure 2 for the KdpBN domain. The protein bands below the 17 kDa band of KdpBN are degradation products (Figure 2). In both cases, the protein yield was

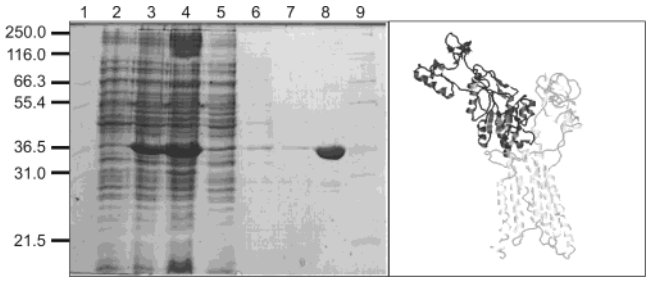

FIGURE 1: Purification of the H4H5 loop. In the left panel, the H4H5 loop was purified using Ni-NTA affinity chromatography. Aliquots from different purification steps were subjected to SDS−PAGE. Each lane was loaded with 5 μL of the following samples: (1) molecular mass standard (kDa); (2) whole cell extract of uninduced cells; (3) whole cell extract of induced cells; (4) soluble fraction after cell lysis; (5) flow-through fraction; (6) washing step I; (7) washing step II; (8) elution fraction; (9) molecular mass standard. The purification was carried out as described in Experimental Procedures. The binding buffer contained 10 mM imidazole, the washing buffer 60 mM imidazole, and the elution buffer was supplemented with 250 mM imidazole. The gel was stained with Coomassie blue. The right panel shows the H4H5 loop according to the KdpB model. Amino acids contributing to the H4H5 loop (Met282−Gln567) according to a 3D KdpB model are in gray. The structural model is based on the Ca^{2+}-ATPase structure (1EUL.pdb) (*18*) and modeling was carried out using the programs "What If" (*44*) and "O" (*45*).

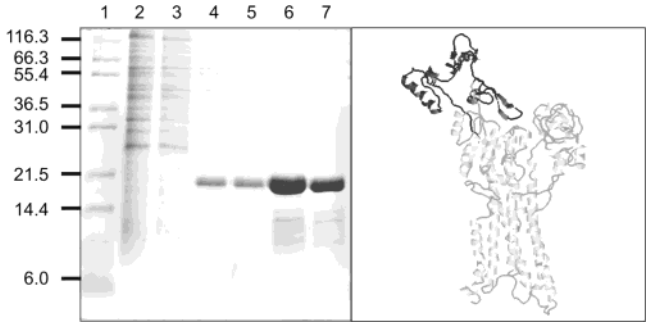

FIGURE 2: Purification of the KdpBN domain. In the left panel, the KdpBN domain was purified using Ni−NTA affinity chromatography. Aliquots from different purification steps were subjected to SDS−PAGE. Each lane was loaded with 5 μL of the following samples: (1) molecular mass standard (kDa); (2) flow-through fraction; (3) washing step I; (4) washing step II; (5) washing step III; (6) elution fraction I; (7) elution fraction II. The purification was carried out as described in Experimental Procedures. Washing step I was performed in the presence of 10 mM imidazole, and washing steps II and III were carried out in the presence of 60 mM imidazole. The elution buffer contained 250 mM imidazole. The gel was stained with Coomassie blue. The right panel shows the KdpBN domain according to the KdpB model. Amino acids contributing to the KdpBN domain (Asn316−Gly451) are in gray. Note that the modeling of this domain was not possible according to the Ca^{2+}-ATPase structure, since KdpBN is roughly 100 amino acids smaller in size.

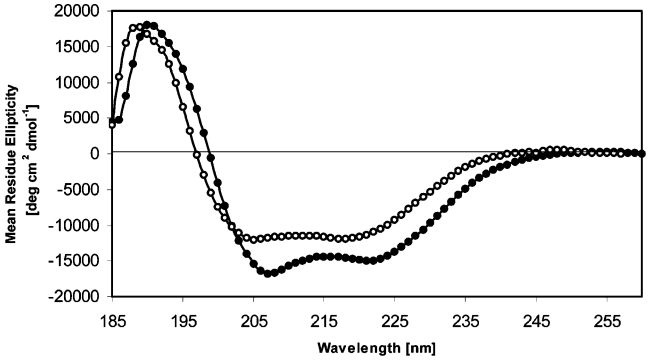

FIGURE 3: CD spectra of the purified H4H5 loop. H4H5 was purified and dialyzed against 50 mM potassium phosphate buffer, pH 7.8. The protein concentration was 0.5 mg mL^{-1}. H4H5 was analyzed without any additives (●) and in the presence of 1 mM ATP (○). Fifty spectra were acquired, coadded, and corrected by the corresponding buffer spectra. The data were converted to mean residue ellipticity using an average amino acid mass of 115 Da.

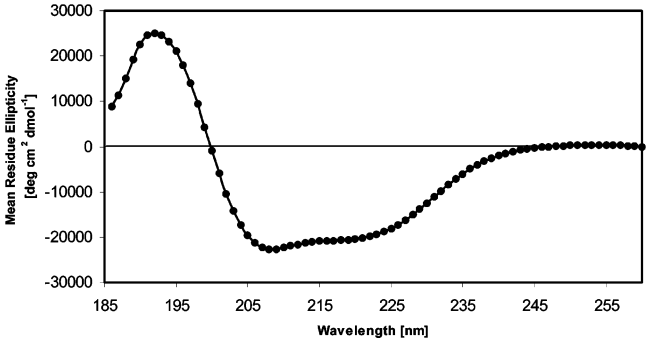

FIGURE 4: CD spectra of the purified KdpBN. KdpBN was purified and dialyzed against 50 mM potassium phosphate buffer, pH 7.8. The protein concentration was 1.8 mg mL^{-1}. KdpBN was analyzed without any additives (●) and in the presence of 15 μM FITC (data not shown, since the curve is indistinguishable from that of the unmodified protein). Fifty spectra were acquired, coadded, and corrected by the corresponding buffer spectra. The data were converted to mean residue ellipticity using an average amino acid mass of 115 Da.

between 10 and 20 mg of purified protein per liter of LB medium. Both proteins could also be obtained using minimal medium for cell growth, where comparably less degradation occurred. With the use of an Amicon cell, the H4H5 protein could be concentrated up to 2 mg mL^{-1}, whereas in case of the KdpBN domain, 20 mg mL^{-1} was achieved.

CD Spectroscopy. The secondary structure of the recombinant proteins was analyzed using CD spectroscopy. The data sets were converted to mean residue ellipticity using a mean residue mass of 115 Da and deconvoluted by the self-consistent method (*25*). The spectra of H4H5 and KdpBN are shown in Figures 3 and 4, respectively. Both proteins showed minima that are indicative of an α-helical structure. The minima for the H4H5 loop were at 207 and 221 nm (Figure 3) and those for the KdpBN domain at 208 and 219 nm (Figure 4). For the H4H5 loop 38% α-helix and 13% β-sheet and for the KdpBN domain 40% α-helix and 10% β-sheet were calculated. Although this method does not allow a detailed structural analysis, the data revealed that the H4H5 loop and the KdpBN domain are properly folded. Upon binding of ATP (1 mM) to H4H5, the minima were shifted to 208 and 218 nm, but the overall secondary structure was not altered. The FITC-labeled (15 μM) KdpBN displayed no changes in the CD spectrum at all.

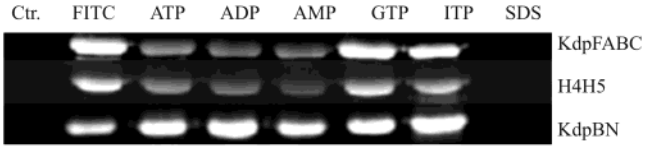

FIGURE 5: FITC binding to KdpFABC, H4H5, and KdpBN. Purified KdpFABC complex, H4H5 loop, and KdpBN domain were incubated with 15 μM FITC for 30 min at 37 °C. To test the protective effect of nucleotides, the proteins were preincubated with 5 mM of the different nucleotides (as indicated). FITC modification was stopped by addition of Laemmli SDS sample buffer, and the mixture was subjected to SDS−PAGE. The protein bands were visualized under UV light (366 nm). The upper lane shows only the KdpB subunit of the native KdpFABC complex. For unspecific binding, protein was incubated with 1% SDS at 80 °C for 5 min prior FITC addition. A fluorescent control with untreated protein (Ctr) was added to show that the protein does not exhibit autofluorescence. FITC-modified protein (FITC) shows the modification without any additives, except FITC.

FITC Modification. Many of the known P-type ATPases (noteworthy exceptions are the heavy metal transporting ATPases) share the KGXXE/D motif in the nucleotide binding domain. The lysine residue within this motif was shown to bind FITC in the case of the Na^+,K^+-ATPase (*26*), the Ca^{2+}-ATPase (*27*), the H^+-ATPase (*28*), and the H^+,K^+-ATPase (*29*). Previously, it was demonstrated that a similar motif in KdpB, 395-KGSVD-399, is probably the FITC binding motif within the Kdp-ATPase (*30*). Figure 5 summarizes the results obtained for FITC labeling of the two soluble domains in comparison with the KdpB subunit of the intact complex. For the H4H5 loop, it can clearly be seen that the FITC modification can be prevented by adenosine nucleotides in the same manner as observed for the Kdp-FABC complex (*30*). GTP and ITP mediate no protective effect. Interestingly, the KdpBN domain is labeled with FITC as expected, but all nucleotides failed to protect against FITC modification. Since ATP binding is reversible and FITC labeling is a covalent modification, we checked whether short incubation times (0.5−30 min) would give different results. Even after 0.5 min, no protective effect of either ATP or AMP was found (data not shown). Unspecific labeling with FITC can be ruled out in all three cases, since SDS-denatured proteins could not be labeled any more by FITC, also indicating that FITC modification obligatorily needs a properly folded protein.

TNP-Nucleotide Binding Studies. TNP-nucleotides are a useful tool in the characterization of ATP binding sites, since these nucleotide derivatives increase their fluorescence at 545 nm drastically upon binding to a appropriate binding site. We used TNP-ATP, TNP-ADP, and TNP-AMP to test nucleotide binding to the H4H5 loop and the KdpBN domain of KdpB. As shown in Figure 6, TNP-ATP binds with an apparent K_d of 18.5 μM. The calculated K_d values for TNP-ADP and TNP-AMP are 24.2 and 52 μM, respectively. TNP-nucleotide binding is only observed in the properly folded state, since no fluorescence increase was observed with SDS-denatured protein (Figure 6). The KdpBN domain also binds the TNP-nucleotides; however, the K_d values are lower compared to those of the H4H5 loop. A total of 1.23 mol of nucleotide binding sites per mole of H4H5 polypeptide chain was calculated using TNP-ATP (Figure 7). The values for TNP-ADP and TNP-AMP were 1.05 and 1.5 mol of binding sites per mole of H4H5. The average value

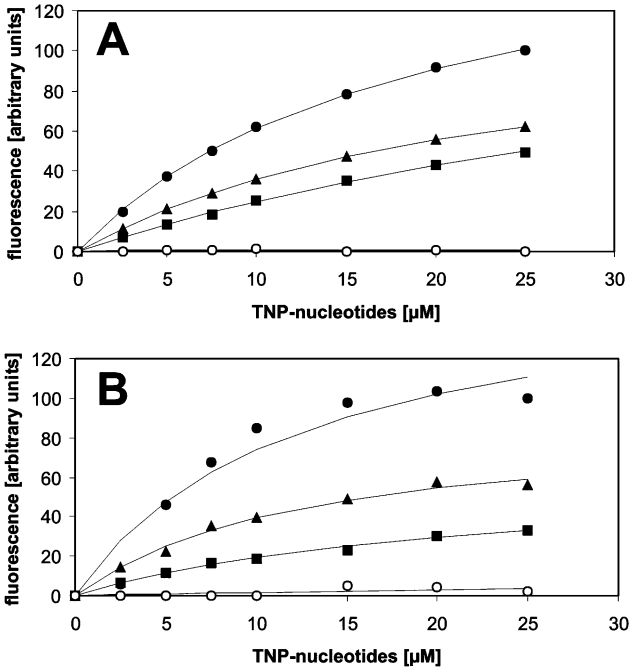

FIGURE 6: Nucleotide binding to H4H5 (A) and KdpBN (B): (●) TNP-ATP; (▲) TNP-ADP; (■) TNP-AMP; (○) denatured. The fluorescence change of TNP-adenosine nucleotides upon binding to H4H5 and KdpBN was measured at 545 nm after excitation at 408 nm. To demonstrate unspecific binding, SDS-denatured proteins were used as a control. Data were fitted to the equation a[TNP-nucleotide]/(b + [TNP-nucleotide]) with a representing the maximum fluorescence change and b the apparent K_d.

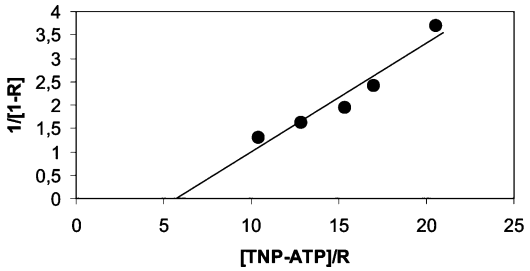

FIGURE 7: Determination of the number of nucleotide binding sites for H4H5. The fraction of fluorescence saturation at each TNP-ATP concentration ($R - F/F_{max}$) was calculated and plotted as $1/(1 - R)$ versus [TNP-ATP]/R. The concentration of TNP-ATP binding sites of H4H5 can be obtained from the relation $1/(1 - R) = K_d^{-1}$[TNP-ATP]/($R-(n/K_d)$) according to Gutfreund (*31*). The data are derived from the TNP-ATP binding curve displayed in Figure 6.

determined for KdpBN was 1.096 mol of nucleotide binding sites per mole of KdpBN. Calculations were performed according to Gutfreund (*31*) and Carvalho-Alves et al. (*32*).

Since TNP-nucleotides are only analogues, it was necessary to perform displacement studies with nucleotides to determine the affinity constants for ATP, ADP, and AMP, respectively. For the displacement studies, the H4H5 loop and the KdpBN domain were preincubated with TNP-ATP at room temperature (see Experimental Procedures) and subsequently titrated with adenosine nucleotides (ATP, ADP, and AMP). The data obtained were fitted as previously described (see Experimental Procedures), and the apparent K_d values were determined (Figure 8). The apparent K_d value for ATP binding to the H4H5 loop was 1.8, for ADP 1.2, and for AMP 1.8 mM. The apparent K_d for ATP binding to

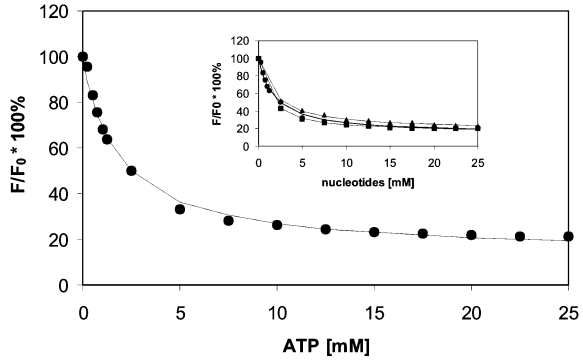

FIGURE 8: TNP-ATP displacement by ATP. Purified H4H5 (5 μM) was incubated with 5 μM TNP-ATP in 20 mM HEPES-Tris, pH 7.8. The recorded fluorescence after addition of 5 μM TNP-ATP was set to 100%. The effect of adenosine nucleotides was monitored following progressive addition of adenosine nucleotides from a stock solution. For reasons of clarity, the curves for ATP (●), ADP (■), and AMP (▲) are shown in the inset only, since they follow the same kinetics. To take dilution factors into account, controls with buffer without nucleotide were titrated. The data are shown as percentage decrease in fluorescence.

KdpBN was 1.3, for ADP 1.7, and for AMP 2.2 mM (data not shown). All displacements were competitive, indicating that ATP, ADP, and AMP bind to the same binding site as TNP-ATP does in the KdpBN domain. It is remarkable that AMP binds with similar kinetics to the nucleotide binding domain of KdpB as ATP, which represents an apparent difference between the Kdp modules and similar domains of P2-type ATPases (*34*, *40*). In case of the Wilson's disease protein, it was reported that AMP and ATP are able to compete with TNP-ATP for binding to the isolated catalytic loop (*33*). However, it should be noted that we found no additive effect of ATP after titration with AMP, as described for the catalytic loop of the Wilson's disease protein (*33*).

Hydrolytic Activity of the H4H5 Loop. More direct evidence for the binding of ATP by the H4H5 loop was obtained by measuring ATP hydrolysis. The specific activity was around 7 nmol mg^{-1} min^{-1} (data not shown). This activity is 700−1400-fold lower compared to the full-length protein in the native complex (5−10 μmol mg^{-1} min^{-1}). However, the specific activity is in the same range as determined for the soluble cytoplasmic loop of the Wilson's disease protein (ATP7B) (*33*), which has a similar domain size. P-type ATPases hydrolyze the small pseudosubstrate pNPP, which was also recently shown for the native KdpFABC complex (*30*). In case of the KdpB H4H5 loop, the activity is 7-fold lower compared to that of the full-length protein (*30*) (Figure 9).The activity was not inhibited by *ortho*-vanadate and not stimulated by potassium ions (data not shown), the implications of which are discussed.

DISCUSSION

The modular design of membrane proteins allows the preparation and characterization of functional domains, which are more amenable to structural analysis than intact proteins. Since the KdpFABC complex from *E. coli* has not only a rather unique subunit composition but also a very small nucleotide binding domain compared to other P-type ATPases, we have set out to determine the structure of the large cytoplasmic loop (H4H5) of the KdpB subunit by NMR spectroscopy. As a first step in this direction, we have

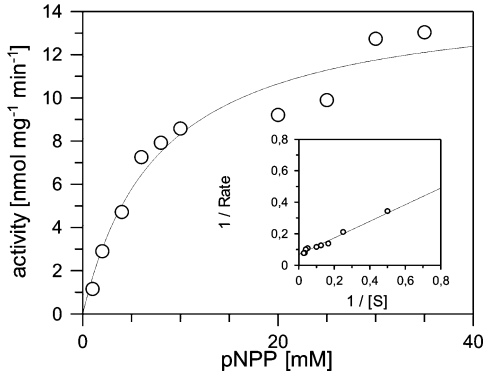

FIGURE 9: pNPPase activity of the H4H5 loop. In a total reaction volume of 100 μL, 5 μg of protein was incubated in 20 mM HEPES-Tris buffer, pH 7.8, containing 15 mM $MgCl_2$. The reaction was started by addition of 15 mM pNPP and stopped after 30 min by addition of 0.1 M NaOH. The production of *p*-nitrophenolate was determined using a *p*-nitrophenolate standard curve. K_M and V_{max} values were calculated from the double reciprocal plot (insert).

isolated and biochemically characterized the H4H5 and the KdpBN domains of KdpB.

To test whether these two recombinant proteins are properly folded, we have applied circular dichroism (CD) spectroscopy. The spectra obtained suggest a mainly α-helical structure for both proteins (Figures 3 and 4). A similar CD spectrum was reported for the catalytic loop of the Na^+,K^+-ATPase (*34*) with minima at 206 and 221 nm. The calculated secondary structure values were 23% α-helix and 27% antiparallel β-sheet. CD-spectroscopic analysis of the large cytoplasmic loop of the SERCA pump revealed an α-helical content of 23% and a β-strand content of 21% (*32*). The differences in the α-helical and the β-sheet content between the sodium pump loop and the SERCA pump loop, on one hand, and the KdpB domains, on the other hand, probably reflect the differences within the N-domain, which is smaller in size in case of the KdpB polypeptide and may contain less β-sheet content in comparison to type II P-type ATPases.

P-type ATPases containing the FITC binding motif KGXXE/D are often examined using FITC labeling. It was shown that FITC binds in or near the ATP binding site. Furthermore, it was demonstrated that FITC fluorescence is altered by adding substrates reflecting certain steps within the reaction cycle of the protein. Interestingly, the covalent modification of P-type ATPases by FITC is only observed with nondenatured protein. Since FITC binding to the intact KdpB subunit was shown recently (*30*), we used this approach to test the folding of and the nucleotide binding to the H4H5 loop and the KdpBN protein. Both proteins were able to bind FITC, although only the H4H5 loop exhibited the same protective effect of nucleotides toward FITC modification as the native full-length KdpB protein within the KdpFABC complex (Figure 5). In contrast to the Na^+,K^+-ATPase (*34*), both the Kdp-ATPase and the H4H5 loop were able to bind AMP with high affinity as judged by the protective effect of AMP toward FITC. Moreover, nucleotides that do not bind with high affinity to the Kdp-ATPase, such as GTP and ITP, were not able to compete with FITC (Figure 5). These results clearly show that the recombinant H4H5 loop not only is able to bind nucleotides but also forms a proper binding pocket, giving rise to selectivity, as does the native loop in the full-length protein. Furthermore, the substrate specificity of KdpB shows clear differences to other P-type ATPases of the type II class, such as the Na^+,K^+-ATPase. The KdpBN domain could also be labeled with FITC, consequently showing that the FITC-binding site is indeed within this domain. However, in contrast to the H4H5 loop, nucleotides had no protective effect. Therefore, it is conceivable that FITC and nucleotides bind simultaneously to the isolated KdpBN domain. This could be possible if the fluorescein moiety of FITC is bent somewhat outward of the binding pocket providing space for the adenine ring to enter as well.

The determination of nucleotide-binding affinities using TNP-nucleotides of full-length P-type ATPases (*35*−*38*) and separately synthesized modules was achieved in several cases (*33*, *34*, *39*, *40*). TNP-nucleotides bind also with high affinity to the H4H5 loop and the KdpBN domain of the Kdp-ATPase (Figure 6). The calculated affinity constants for TNP-ATP (18.5 μM for the H4H5 loop and 12.2 μM for the KdpBN domain) are lower compared to those for other P-type ATPase loops. The TNP-ATP K_d value for the Na^+,K^+-ATPase loop was 3.2 μM (*34*), for the Ca^{2+}-ATPase loop 1.9 μM (*40*), for the H^+-ATPase loop 6.5 μM (*39*), and 1.89 μM in the case of the Wilson's disease protein loop (*33*). Interestingly, TNP-ATP bound with higher affinity to the KdpBN domain than to the H4H5 loop, suggesting that in the case of KdpBN the binding pocket might be more accessible for the nucleotide. The K_d values for the H4H5 loop and the KdpBN domain decreased as TNP-ATP > TNP-ADP >TNP-AMP for both the KdpBN domain and the H4H5 loop. An even more convincing evidence for the binding of adenosine nucleotides stems from the observation that ATP is able to competitively displace TNP-ATP from its binding site. These experiments revealed that differences exist between the Kdp-ATPase and the P2-type ATPases such as Na^+,K^+-ATPase (*34*) and the Ca^{2+}-ATPase (*40*), where AMP was shown not to bind or to bind only with low affinity compared to ATP. Similar to the Kdp-ATPase modules, the catalytic loop of the Wilson's disease protein (P1-type ATPase) exhibited AMP binding. However, in case of the Wilson's disease protein AMP could quench the TNP-ATP fluorescence to a smaller extent compared to ATP. Furthermore, when saturation with AMP was reached, the TNP-ATP fluorescence could be further decreased upon addition of ATP, suggesting two binding sites in case of the Wilson's disease protein (*33*). We have not observed these kinds of effects with the isolated Kdp domains. Although the Kdp-ATPase and the Wilson's disease protein share a similar domain size and are grouped together as P1-type ATPases, there seem to be significant differences between both enzymes with respect to their nucleotide binding properties. At first glance, the affinity for ATP toward H4H5 (1.8 mM) and KdpBN (1.3 mM) seems to be quite low. One reason for the low affinity constants may be that the isolated domains are in an E2-like conformation, as it was suggested for these domains before (*33*, *34*, *39*, *40*). A recent study on the copper transporting ATPase ATP7B (*43*) showed that ATP binds to the isolated domains of this P1b-ATPase with much higher affinity (70−80 μM) than to the P2-ATPase N-domains (0.7−5 mM). The apparent binding affinities of ATP to the isolated Kdp domains are similar to those of the P2-type ATPases but distinct from those of the heavy metal-transporting ATPases (P1b-type). Differences in the ATP

affinity found with different P-type ATPases and their corresponding loops seem to reflect differences in the structure of the nucleotide binding site. The plasma membrane H^+-ATPase exhibits lower affinities for both TNP-ATP and ATP compared to the Na^+,K^+-ATPase and the SERCA pump, while the affinities determined for the Kdp-ATPase are even lower. Interestingly, in comparison to the type II class ATPases, the size of the nucleotide binding domain of the H^+-ATPase and the Kdp-ATPase is smaller, which may be responsible for the different substrate affinities. Finally, the molar ratio of bound TNP-nucleotides to the H4H5 loop and the KdpBN domain clearly support the one binding site hypothesis for P-type ATPases. Furthermore, nucleotide binding studies on isolated cytosolic domains stress the importance of the transmembrane domains for the generation of a high-affinity ATP binding site.

Hydrolytic activity was already reported for H4H5 of the Na^+,K^+-ATPase loop (*41*, *42*) and the Wilson's disease protein (*33*). Also for the H4H5 loop of KdpB, we were able to measure a low ATP hydrolyzing activity with a specific activity of 7 nmol mg^{-1} min^{-1}, which was lower than that reported for the H4H5 loop of the Wilson's disease protein (67.6 nmol mg^{-1} min^{-1}) (*33*). In addition, we measured the hydrolysis of pNPP (Figure 9), which was recently described for the KdpFABC complex (*30*). The measured specific activity was in the same range as the ATPase activity (15 nmol mg^{-1} min^{-1}). Compared to the pNPP hydrolysis reported for the H4H5 loop of the Na^+,K^+-ATPase (2−3 nmol mg^{-1} h^{-1}) (*42*), the activity of the H4H5 loop of KdpB is quite high. The hydrolytic activity of the H4H5 loop provides convincing evidence in favor for the formation of a properly folded subdomain of KdpB. The pNPPase activity of H4H5 was not stimulated by potassium ions. This result was expected, since subunit KdpA, which binds K^+ , is missing. Interestingly, the pNPPase activity of H4H5 was, in contrast to that for the full-length protein (*30*), not inhibited by vanadate. A plausible explanation might be that the H4H5 loop is not phosphorylated after pNPP hydolysis and hence lacks the transition state that is mimicked by *ortho*-vanadate.

The results presented in this report provide evidence for the independent folding of the large cytoplasmic domain (H4H5) and the nucleotide binding domain (KdpBN), which comprises one module within the catalytic loop. It was shown that FITC binds to the intact recombinant proteins and that in the case of the H4H5 loop adenosine nucleotides prevent FITC modification. The fact that this was not observed for the KdpBN domain and the fact that the TNP-nucleotides bind with higher affinity to KdpBN compared to H4H5 may reflect a more open binding site, which in turn is more accessible to FITC and nucleotides. For the intact H4H5 loop, the accession to the binding site may be blocked by FITC, while in case of KdpBN, FITC modification might be not sufficient to prevent additional nucleotide binding. Analysis of the catalytic part of the KdpFABC complex underlines the similarities between the Kdp-ATPase and other P-type ATPases with respect to their catalytic properties. However, the existence of the FITC binding motif and the relatively low binding affinities for ATP clearly separate the Kdp-ATPase from the heavy-metal ATPases and suggest a closer evolutionary relationship of KdpB to the H^+-ATPases.

ACKNOWLEDGMENT

We are grateful to Dr. Jörg-Christian Greie for his help with the CD spectroscopy, Drs. Siegfried Engelbrecht and Michael Gassel for construction of the KdpB homology model, and Brigitte Herkenhoff-Hesselmann for experienced technical assistance.

REFERENCES

1. Epstein, W. (1986) Osmoregulation by potassium transport in *Escherichia coli*, *FEMS Microbiol. Rev. 39*, 73−78.
2. Stumpe, S., Schlösser, A., Schleyer, M., and Bakker, E. P. (1996) K^+ circulation across the prokaryotic cell membrane: K^+ uptake systems. In: *Handbook of Biological Physics* (Konings, W. N., Kaback, H. R., and Lolkema, J. S., Eds.) Vol. 2, pp 473−499, Elsevier Science, Amsterdam.
3. Rhoads, D. B., Waters, F. B., and Epstein, W. (1976) Cation transport in *Escherichia coli*. VIII. Potassium transport mutants, *J. Gen. Physiol. 67*, 325−341.
4. Epstein, W. (1985) The Kdp system: a bacterial K^+ transport ATPase, *Curr. Top. Membr. Transp. 23*, 153−175.
5. Laimins, L. A., Rhoads, D. B., Altendorf, K., and Epstein, W. (1978) Identification of the structural proteins of an ATP-driven potassium transport system in *Escherichia coli*, *Proc. Natl. Acad. Sci. U.S.A. 75*, 3216−3219.
6. Lutsenko, S., and Kaplan, J. H. (1995) Organization of P-Type ATPases: Significance of structural diversity, *Biochemistry 34*, 15607−15613.
7. Axelsen, K. B., and Palmgreen, M. G. (1998) Evolution of substrate specificities in the P-type ATPase superfamily, *J. Mol. Evol. 46*, 84−101.
8. Altendorf, K., and Epstein, W. (1996) The Kdp-ATPase of *Escherichia coli*, In: *Biomembranes (ATPases)* (Lee, A. G., ed.) Vol. 5, pp 403−420, JAI Press Inc., Greenwich, London.
9. Altendorf, K., Gassel, M., Puppe, W., Möllenkamp, T., Zeeck, A., Boddien, C., Fendler, K., Bamberg, E., and Dröse, S. (1998) Structure and function of the Kdp-ATPase of *Escherichia coli*, *Acta Physiol. Scand. 163*, 137−146.
10. Siebers, A., and Altendorf, K. (1989) Characterization of the phosphorylated intermediate of the K^+-translocating Kdp-ATPase from *Escherichia coli*, *J. Biol. Chem. 264*, 5831−5838.
11. Puppe, W., Siebers, A., and Altendorf, K. (1992) The phosphorylation site of the Kdp-ATPase of *Escherichia coli*: site-directed mutagenesis of the aspartic acid residues 300 and 307 of the KdpB subuni, *Mol. Microbiol. 6*, 3511−3520.
12. Serrano, R. (1988) Structure and function of proton translocating ATPase in plasma membranes of plants and fungi, *Biochim. Biophys. Acta 947*, 1−28.
13. Buurman, E. T., Kim, K.-T., and Epstein, W. (1995) Genetic evidence of two sequentially occupied K^+ binding sites in the Kdp transport ATPase, *J. Biol. Chem. 270*, 6678−6685.
14. Durell, S. R., Bakker, E. P., and Guy, H. R. (2000) Does the KdpA subunit from the high affinity K^+-translocating P-type Kdp-ATPase have a structure similar to that of K^+ channels? *Biophys. J. 78*, 188−199.
15. Dorus, S., Mimura, H., and Epstein, W. (2001) Substrate-binding clusters of the K^+-transporting Kdp ATPase of *Escherichia coli* investigated by amber suppression scanning mutagenesis, *J. Biol. Chem. 276*, 9590−9598.
16. Van der Laan, M., Gassel, M., and Altendorf, K. (2002) Characterization of amino acid substitutions in KdpA, the K^+-binding and -translocating subunit of the KdpFABC complex of *Escherichia coli*, *J. Bacteriol. 184*, 5491−5494.
17. Bertrand, J., Altendorf, K., and Bramkamp, M. (2004) Amino acid substitutions in the putative selectivity filter regions III and IV in KdpA alter ion selectivity of the KdpFABC complex from *Escherichia coli*, *J. Bacteriol. 186*, 5519−5522.
18. Toyoshima, C., Nakasako, M., Nomura, H., and Ogawa, H. (2000) Crystal structure of the calcium pump of sarcoplasmic reticulum at 2.6 Å resolution, *Nature 405*, 647−655.
19. Toyoshima C., and Nomura, H. (2002) Structural changes in the calcium pump accompanying the dissociation of calcium, *Nature 418*, 605−611.

20. Laemmli, U.K. (1970) Cleavage of structural proteins during the assembly of the head of bacteriophage T4, *Nature 227*, 680−685.
21. Blum, H., Beier, H., and Gross, H. J. (1987) Improved silver staining of plant proteins, RNA and DNA in polyacrylamide gels, *Electrophoresis 8*, 93−99.
22. Weber, K., and Osborn, M. (1969) The reliability of molecular weight determinations by dodecyl sulfate-polyacrylamid gel electrophoresis, *J. Biol. Chem. 244*, 4406−4412.
23. Siebers, A., and Altendorf, K. (1988) The K^+-translocating Kdp-ATPase from *Escherichia coli*. Purification, enzymatic properties and production of complex- and subunit-specific antisera, *Eur. J. Biochem. 178*, 131−140.
24. Bramkamp, M., Gassel, M., Herkenhoff-Hesselmann, B., Bertrand, J., and Altendorf K. (2003) The *Methanocaldococcus jannaschii* protein Mj0968 is not a P-type ATPase, *FEBS Lett. 543*, 31−36.
25. Sreerama, N., and Woody, R. W. (1994) Protein secondary structure from circular dichroism spectroscopy. Combining variable selection principle and cluster analysis with neural network, ridge regression and self-consistent methods, *J. Mol. Biol. 242*, 497−507.
26. Farley, R. A., Tran, C. M., Carilli, C. T., Hawke, D., and Shively, J. E. (1984) The amino acid sequence of a fluorescein-labeled peptide from the active site of (Na,K)-ATPase, *J. Biol. Chem. 259*, 9532−9535.
27. Pick, U., and Bassilian, S. (1981) Modification of the ATP binding site of the Ca^{2+} -ATPase from sarcoplasmic reticulum by fluorescein isothiocyanate, *FEBS Lett. 123*, 127−130.
28. Pardo, J. P., and Slayman, C. W. (1988) The fluorescein isothiocyanate-binding site of the plasma-membrane H^+-ATPase of *Neurospora crassa*, *J. Biol. Chem. 263*, 18664−18668.
29. Saccomani, G., and Mukidjam, E. (1987) Papain fragmentation of the gastric ($H^+ + K^+$)-ATPase, *Biochim. Biophys. Acta 912*, 63−73.
30. Bramkamp, M., Gassel, M., and Altendorf, K. (2004) FITC binding site and *p*-nitrophenyl phosphatase activity of the Kdp-ATPase of *Escherichia coli*, *Biochemistry 43*, 4559−4567.
31. Gutfreund, H. (1972) *Enzymes, physical principles*, p 71, Wiley-Inter-Science, London.
32. Carvalho-Alves, P. C., Hering, V. R., Oliveira, J. M., Salinas, R. K., and Verjovski-Almeida, S. (2000) Requirement of the hinge domain for dimerization of Ca^{2+}-ATPase large cytoplasmic portion expressed in bacteria, *Biochim. Biophys. Acta. 1467*, 73−84.
33. Tsivkovskii, R., MacArthur, B. C., and Lutsenko, S. (2001) The Lys1010-Lys1325 fragment of the Wilson's disease protein binds nucleotides and interacts with the N-terminal domain of this protein in a copper-dependent manner, *J. Biol. Chem. 276*, 2234−2242.
34. Gatto, C., Wang, A. X., and Kaplan, J. H. (1998) The M4M5 cytoplasmic loop of the Na, K.-ATPase, overexpressed in *Escherichia coli*, binds nucleoside triphosphates with the same selectivity as the intact native protein, *J. Biol. Chem. 273*, 10578−10585.
35. Moczydlowski, E. G., and Fortes, P. A. (1981a) Characterization of 2′,3′-O-(2,4,6-trinitrocyclohexadienylidine)adenosine 5′-triphosphate as a fluorescent probe of the ATP site of sodium and potassium transport adenosine triphosphatase. Determination of nucleotide binding stoichiometry and ion-induced changes in affinity for ATP, *J. Biol. Chem. 256*, 2346−2356.
36. Moczydlowski, E. G., and Fortes, P. A. (1981) Inhibition of sodium and potassium adenosine triphosphatase by 2′,3′-O-(2,4,6-trinitrocyclohexadienylidene) adenine nucleotides. Implications for the structure and mechanism of the Na:K pump, *J. Biol. Chem. 256*, 2357−2366.
37. Watanabe, T., and Inesi, G. (1982) The use of 2′,3′-O-(2,4,6-trinitrophenyl) adenosine 5′-triphosphate for studies of nucleotide interaction with sarcoplasmic reticulum vesicles, *J. Biol. Chem. 257*, 11510−11516.
38. Faller, L. D. (1989) Competitive binding of ATP and the fluorescent substrate analogue 2′,3′-O-(2,4,6-trinitrophenylcyclohexadienylidine) adenosine 5′-triphosphate to the gastric H^+,K^+-ATPase: evidence for two classes of nucleotide sites, *Biochemistry. 28*, 6771−6778.
39. Capieaux, E., Rapin, C., Thines, D., Dupont, Y., and Goffeau, A. (1993) Overexpression in *Escherichia coli* and purification of an ATP-binding peptide from the yeast plasma membrane H^+-ATPase, *J. Biol. Chem. 268*, 21895−21900.
40. Moutin, M. J., Cuillel, M., Rapin, C., Miras, R., Anger, M., Lompre, A. M., and Dupont, Y. (1994) Measurements of ATP binding on the large cytoplasmic loop of the sarcoplasmic reticulum Ca^{2+}-ATPase overexpressed in *Escherichia coli*, *J. Biol. Chem. 269*, 11147−11154.
41. Obsil, T., Merola, F., Lewit, B. A., and Amler, E. (1998) The isolated H4−H5 cytoplasmic loop of Na, K.-ATPase overexpressed in *Escherichia coli* retains its ability to bind ATP, *Gen. Physiol. Biophys. 17* (Suppl 1), 52−55.
42. Tran, C. M., and Farley, R. A. (1999) Catalytic activity of an isolated domain of Na,K-ATPase expressed in *Escherichia coli*, *Biophys. J. 77*, 258−266.
43. Morgan, C. T., Tsivkovskii, R., Kosinsky, Y. A., Efremov, R. G., and Lutsenko, S. (2004) The distinct functional properties of the nucleotide-binding domain of ATP7B, the human copper-transporting ATPase. Analysis of the wilson disease mutations E1064A, H1069Q, R1151H, and C1104F, *J. Biol. Chem.*, epub ahead of print.
44. Vriend, G. (1990) WHAT IF: A molecular modeling and drug design program, *J. Mol. Graphics 8*, 52−56.
45. Jones, T. A., and Kjeldgaard, M. (1998) *Essential 'O', software manual*, p 178, Uppsala, Sweden.

BI048727D